UC Riverside

UC Riverside Previously Published Works

Title

Synthesis of Formate from CO2 Gas Catalyzed by an O2-Tolerant NAD-Dependent Formate Dehydrogenase and Glucose Dehydrogenase

Permalink

https://escholarship.org/uc/item/41j296sh

Journal

Biochemistry, 58(14)

ISSN

0006-2960

Authors

Yu, Xuejun
Niks, Dimitri
Ge, Xin
et al.

Publication Date

2019-04-09

DOI

10.1021/acs.biochem.8b01301

Peer reviewed

eScholarship.org Powered by the California Digital Library
University of California

Biochemistry

Article

Cite This: *Biochemistry* 2019, 58, 1861−1868

pubs.acs.org/biochemistry

Synthesis of Formate from CO_2 Gas Catalyzed by an O_2-Tolerant NAD-Dependent Formate Dehydrogenase and Glucose Dehydrogenase

Xuejun Yu,[†,‡] Dimitri Niks,[†] Xin Ge,[§] Haizhou Liu,[§] Russ Hille,[*,†] and Ashok Mulchandani[*,§,∥]

[†]Department of Biochemistry, [‡]Department of Bioengineering, [§]Department of Chemical and Environmental Engineering, [∥]Materials Science and Engineering Program, University of California Riverside, 900 University Avenue, Riverside, California 92521, United States

ABSTRACT: Direct biocatalytic conversion of CO_2 to formic acid is an attractive means of reversibly storing energy in chemical bonds. Formate dehydrogenases (FDHs) are a heterogeneous group of enzymes that catalyze the oxidation of formic acid to carbon dioxide, generating two protons and two electrons. Several FDHs have recently been reported to catalyze the reverse reaction, i.e., the reduction of carbon dioxide to formic acid, under appropriate conditions. The main challenges with these enzymes are relatively low rates of CO_2 reduction and high oxygen sensitivity. Our earlier studies (Yu et al. (2017) *J. Biol. Chem.* **292**, 16872−16879) have shown that the FdsABG formate dehydrogenase from *Cupriavidus necator* is able to effectively catalyze the reduction of CO_2, using NADH as a source of reducing equivalents, with a good oxygen tolerance. On the basis of this result, we have developed a highly thermodynamically efficient and cost-effective biocatalytic process for the transformation of CO_2 to formic acid using FdsABG. We have cloned the full-length soluble formate dehydrogenase (FdsABG) from *C. necator* and expressed it in *Escherichia coli* with a His-tag fused to the N terminus of the FdsG subunit; this overexpression system has greatly simplified the FdsABG purification process. Importantly, we have also combined this recombinant *C. necator* FdsABG with another enzyme, glucose dehydrogenase, for continuous regeneration of NADH for CO_2 reduction and demonstrated that the combined system is highly effective in reducing CO_2 to formate. The results indicate that this system shows significant promise for the future development of an enzyme-based system for the industrial reduction of CO_2.

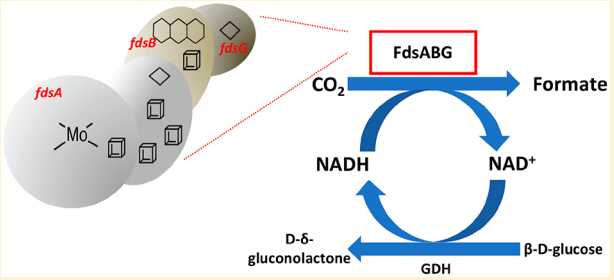

The increasing level of carbon dioxide in the atmosphere is a matter of global concern, given the serious environmental and climate implications. An attractive solution is the utilization of the abundantly available "waste" carbon dioxide as a feedstock to produce useful chemicals and liquid fuels.[1] In recent years, formic acid has become a promising liquid fuel, a hydrogen energy carrier with advantages of a high volumetric capacity (53 g H_2/L), low toxicity, and flammability under ambient conditions as well as its usefulness as an important feedstock for the synthesis of other valuable chemicals.[1−4] A number of heterogeneous catalysts, homogeneous catalysts, electrocatalysts, and photocatalysts have been investigated for the conversion of carbon dioxide to formic acid.[3,5] The systems that have been developed to date, however, exhibit a low selectivity and yield and, in using H_2 as a reductant, require a high temperature and/or high pressure, or high electrochemical overpotentials.[3,6,7] In comparison, biocatalysts for the reduction of CO_2 have the advantage of operating under mild reaction conditions: room temperature, ambient pressure, and neutral pH.[5] Thus, direct conversion of CO_2 to formic acid through biocatalysis is a very attractive option.

Formate dehydrogenases (FDHs) are a heterogeneous and broadly distributed group of enzymes that catalyze the oxidation of formic acid to carbon dioxide, while generating two protons and a pair of reducing equivalents.[8] FDHs can be classified into three categories: metal-independent/NAD(P)$^+$-dependent formate dehydrogenases, metal-containing/NAD(P)$^+$-independent formate dehydrogenases, and metal-containing/NAD(P)$^+$-dependent formate dehydrogenases.[8] Several FDHs have been reported to be able to catalyze the reverse reaction, which is the reduction of carbon dioxide to formic acid under the appropriate conditions.[9] FDH from the yeast *Candida boidinii* (CbFDH) and FDH from bacteria *Thiobacillus* sp. KNK65MA (TsFDH) are examples of metal-independent/NAD(P)$^+$-dependent FDHs.[10] CbFDH, in particular, has been widely investigated for its ability to reduce CO_2 in various ways, including enzymatic cascade and electrochemical or photochemical reactions.[11−14] However, the problem with this and related enzymes is that the CO_2-reducing activity is very low (k_{cat} for TsFDH reported as 0.318 s^{-1} and k_{cat} for CbFDH reported as 0.015 s^{-1}).[10] In comparison, the metal-dependent/NAD(P)$^+$-independent

Received: December 21, 2018
Revised: March 5, 2019
Published: March 6, 2019

Downloaded via UNIV OF CALIFORNIA RIVERSIDE on April 15, 2019 at 16:34:29 (UTC).
See https://pubs.acs.org/sharingguidelines for options on how to legitimately share published articles.

ACS Publications © 2019 American Chemical Society

DOI: 10.1021/acs.biochem.8b01301
Biochemistry 2019, 58, 1861−1868

FDHs, containing tungsten or molybdenum in their active sites, have significantly higher rates of CO_2 reduction. FDH1 and FDH2 from *Syntrophobacter fumaroxidans*, for example, have an extremely high CO_2-reducing activity, with k_{cat} values of 2.5×10^3 s^{-1} and 0.2×10^3 s^{-1}, respectively.[15] Unfortunately, these enzymes are extremely oxygen-sensitive, rendering them unsuitable for industrial applications. An oxygen-tolerant and robust enzyme has potential for future industry applications.

The molybdenum-containing/NAD^+-dependent FDH (FdsABG) from the bacterium *Cupriavidus necator* (formerly known as *Ralstonia eutropha*) is an O_2-tolerant, soluble homodimer of trimers, $(\alpha\beta\gamma)_2$, containing seven iron−sulfur clusters as well as the bis(molybdopterin guanine dinucleotide) molybdenum (bis(MGD)Mo) cofactor and FMN.[16−18] This FdsABG is an unusual enzyme among the metal-dependent formate dehydrogenases family because of the following advantageous properties: O_2 tolerance (particularly in the presence of the stabilizing agent nitrite), high water solubility, and the ability to effectively catalyze the reduction of CO_2 using NADH as a terminal electron donor, stoichiometrically generating formate with a k_{cat} of 10 s^{-1}.[18] Since NADH is a very expensive reducing agent (~$1000/mol), recycling is essential for the process to become cost-effective.[19] Regenerating NADH from NAD^+ generated in the course of CO_2 reduction would also help drive the thermodynamically unfavorable reaction toward the generation of formate, thereby improving reaction yields.[11,13,20,21] Therefore, efficient regeneration of NADH is essential for the in vitro CO_2 fixation process to be economically feasible. Regenerating/recycling NADH by the rereduction of NAD^+ using a second enzyme, electrochemically or photochemically, has been reported,[19] although the systems reported to date have relied on highly O_2-sensitive FDHs.

In this study, we report a thermodynamically efficient and cost-effective biocatalytic process for the transformation of CO_2 to formic acid using the FdsABG formate dehydrogenase from *C. necator*. We have cloned the full-length enzyme and expressed it in *Escherichia coli* with a His-tag fused to the N-terminus of the FdsG subunit and analyzed the recombinant protein by electron paramagnetic resonance (EPR) spectroscopy and kinetic analysis to compare it with the native isolated FdsABG from *C. necator*. Finally, and importantly, we have combined this recombinant *C. necator* FdsABG with a commercially available glucose dehydrogenase (Sigma-Aldrich) to promote continuous electron transfer to the reaction, in which CO_2 is converted to formate. This system has the potential to be further developed for industrial applications.

MATERIALS AND METHODS

Materials. All molecular cloning enzymes including Q5 DNA polymerase, T4 DNA ligase, *Bam*HI, and *Kpn*I were purchased from NEB. Glucose dehydrogenase (from *Pseudomonas* sp.), NAD^+, and NADH were purchased from Sigma-Aldrich (St. Louis, MO); argon and CO_2 were procured from Airgas. Other chemicals were purchased from Fisher Scientific.

Cloning. The FdsGBACD gene (gene ID 4248878−4248882) was amplified by polymerase chain reaction (PCR) using *Cupriavidus necator* chromosomal DNA as a template with the respective primers (primers 1 and 2 in Table 1). The 6xHis tag and Xpress Epitope from the original pTrcHisB vector were replaced by a 6xHis-linker-6xHis tag using PCR with the respective primers (primers 3 and 4 in Table 1) to construct a new vector, pTrc12HLB. The PCR-amplified pTrc12HLB DNA fragments were gel-purified, digested with *Bam*HI, and ligated using T4 DNA ligase; the amplified FdsGBACD DNA fragment was gel-purified, digested with *Bam*HI/*Kpn*I, and cloned into both pTrcHisB and pTrc12HLB vector to encode the 6xHis tag and 6xHis-linker-6xHis tag fused to the N-terminus of the FdsG subunit, respectively. The pTrc12HLB-FdsGBACD vector was transformed into *Escherichia coli* DH5α cells for protein expression and purification.

Table 1. Primers Used in the Cloning Work

primer name	DNA sequence
primer 1	5′-CTA GTG GAT CCG CCA GAA ATT TCC CCC CAC GCA CCG-3′
primer 2	5′-ACG ATG GTA CCC TAC TCC AGC ATC GCC CGA TGC C-3′
primer 3	5′-TAT CGA TTA AAT AAG GAG GAA TAA ACC ATG GGT GGA AGC CAC CAC CAC CAC CAC CAC TCT CGG GCT TGG AGA CAT CCT CAA GGG GGT TCT CAT CAC CAC CAC CAT CAC GGG ATG CGG GAT TTA TAT GAT GAC GAT GAC AAG GAT CCA GTC-3′
primer 4	5′-TCT AAG GAT CCG AGC TCG AGA TCT-3′

Protein Expression and Purification. The FdsABG formate dehydrogenase from *C. necator* was expressed in *E. coli* DH5α cells transformed with the pTrc12HLB-FdsGBACD vector containing the FdsGBACD operon encoding the enzyme. Cells were precultured at 37 °C for 7 h in 3 mL of LB medium containing 50 μg/mL ampicillin. The precultures (200 μL) were transferred into 5 mL of LB containing 0.5 mM sodium molybdate and 50 μg/mL ampicillin and grown overnight at 28 °C with shaking. The cells were then inoculated into 2 L of Terrific Broth (TB) medium supplemented with 50 μM isopropyl β-D-1-thiogalactopyranoside (IPTG), 1 mM sodium molybdate, and 50 μg/mL ampicillin and grown additionally for 20−24 h at 28 °C and 160 rpm. Cells were harvested at OD_{600} = 4.2−4.5 by centrifugation for 15 min at 5000*g* and stored at −80 °C.

All protein purification steps were performed at 4 °C. The harvested *E. coli* cells were resuspended in 40 mM KPO_4, 10 mM KNO_3, pH 7.2, containing 1 mM benzamidine, 1 mM sodium fluoride, 0.5 mM PMSF, lysozyme, and DNase I and disrupted by one passage through a French pressure cell at 10 000 psi. Cell supernatant was collected by centrifugation for 45 min at 150 000*g*, followed by a 25% saturation in ammonium sulfate, and centrifugation for an additional 45 min. The supernatant collected from the 25% fraction was then brought to 50% ammonium sulfate saturation and the pellet subsequently recovered by centrifugation for 20 min at >10 000*g*. The pellet containing FdsABG was then dissolved in 50 mM KPO_4, 10 mM KNO_3 and 15 mM imidazole buffer, pH 7.5, containing 1 mM benzamidine, 1 mM sodium fluoride, and 0.5 mM PMSF. The resuspended solution was batched with Ni-NTA agarose (Qiagen) for 1 h. The resin was then washed with a 5-column volume of 50 mM KPO_4, 10 mM KNO_3, and 20 mM imidazole buffer, pH 7.5, followed by 4 more washes with a 5-column volume each of 50 mM KPO_4, 10 mM KNO_3, and 30 mM imidazole buffer, pH 7.5. The bound protein was eluted with a 5-column volume of 50 mM KPO_4, 10 mM KNO_3, and 300 mM imidazole buffer, pH 7.5. The fractions containing FdsABG were then concentrated and loaded onto a Superdex 200 column (GE Healthcare). Size exclusion chromatography primarily separates the FdsABG

DOI: 10.1021/acs.biochem.8b01301
Biochemistry 2019, 58, 1861−1868

from the FdsBG (also synthesized during the induction of plasmid).[22] Sample purity was confirmed with SDS-PAGE. Routine activity assays were performed as previously described[17,18] at 30 °C in 75 mM KPO_4, pH 7.7 with 2 mM NAD^+, and 40 mM sodium formate. Enzyme concentrations were determined using an estimated extinction coefficient at 410 nm of 51 500 M^{-1} cm^{-1} for the oxidized enzyme,[17,23] and activities were calculated with respect to one trimer with a molecular weight of 178 800 Da.[17,18]

Protein Characterization with EPR Spectroscopy. A Mo-containing sample was prepared as previously described.[17] Electron paramagnetic resonance (EPR) spectra were recorded using a Bruker EMX spectrometer equipped with a Bruker ER 4119HS high sensitivity X-band cavity operating WinEPR version 4.33 acquisition software. The temperature was controlled using a Bruker variable temperature unit and liquid nitrogen cryostat. Simulations were performed as previously described.[17]

Enzymatic Reaction Assay. Kinetic assays for FdsABG with formate and NAD^+ as a substrate were performed under aerobic conditions at 30 °C as previously described.[17] To measure the steady-state parameters for the reaction of FdsABG with formate, 75 mM KPO_4, pH 7.7 buffer was used for maintaining the pH. Formate (4 mM) with a range 0−1 mM NAD^+, or 1 mM NAD^+ with a range 0−3 mM formate, were used in these assays, and the results were plotted according to the Michaelis−Menten equation for calculating the k_{cat} values. The kinetic activity of glucose dehydrogenase (GDH) from *Pseudomonas* sp. was measured in 0.1 M phosphate buffer (pH 7.0) at 30 °C supplemented with 40 mM glucose with a range 0−2.5 mM NAD^+, or 2 mM NAD^+ with a range 0−40 mM glucose. Reactions were initiated by addition of 5 nM GDH in 200 μL assays, and the first 60 s after addition of GDH and the first 10 s after addition of FdsABG were used to calculate the initial slopes. The rates of NADH consumption (for FdsABG) or generation (for GDH) were monitored using a UV−vis spectrophotometer at 340 nm (ε = 6220 M^{-1} cm^{-1}). The results were plotted according to the Michaelis−Menten equation for calculating the k_{cat} values.

To monitor the synthesis of formate from CO_2, enzyme cascade reactions in solution were employed. A 20 mL solution containing 20 mM bis-tris propane buffer, 4−50 mM glucose, and 0.5 mM NAD^+ was first saturated with CO_2 and brought to pH 7.0. The reaction was started with injection of GDH and FdsABG at a 1:20 ratio with an argon-purged gas-tight syringe. The reactions were incubated at 30 °C in a water bath with constant mixing. Samples at different time points were removed, and the enzyme was promptly separated via ultrafiltration with Amicon Ultra 4 (Millipore). The filtrate was analyzed by ion chromatography to quantify the amount of formate produced.

Formic Acid Detection. The reaction samples were analyzed by ion chromatography (Dionex DX-120), using a 4 mm × 25 mm Dionex Ionpac AS22 column and 4.5 mM sodium carbonate/1.4 mM sodium bicarbonate as an eluent with a flow rate of 0.86 mL/min. A range of 0−2 mM formic acid dissolved in 20 mM bis-tris propane buffer supplemented with 20 mM glucose was used as a standard for calibration.

RESULTS AND DISCUSSION

Protein Expression and Purification from *E. coli*. In our recent work,[17,18] native FdsABG was purified from the bacterium *C. necator*, requiring a time-consuming culture growth involving about 4 days of preculture and 6 h of mass culture, followed by 2 days of large volume fermentation. Additionally, the FdsABG purification from *C. necator* is also very time-consuming, labor-intensive, and expensive. We have therefore constructed an overexpression system for the cytosolic *C. necator* FdsABG in *E. coli* to simplify both cell growth and protein purification. Purification was simplified via addition of an affinity histidine-tag at the N-terminus of the FdsG subunit. However, protein expression and purification still remained a challenge with regard to protein synthesis, insertion of complex cofactors during expression, and low protein affinity to Ni-NTA resin.

We first expressed FdsABG with 6xHis tag fused to the N-terminus of the FdsG subunit and found that the enzyme was readily expressed by the *E. coli* recombinant system as monitored by the formate/NADH oxidoreductase activity of the supernatant. However, the recombinant protein did not bind to the Ni-NTA resin. We monitored the purification process utilizing a 1 mL HisTrap FF column and an Akta FPLC (GE Healthcare) at 280 nm for total protein quantification and at 450 nm, where FdsABG absorbs.[17] The chromatograms showed that a great amount of the 6xHis-FdsABG eluted from the Ni-NTA column with washing buffer containing only 20 mM imidazole (Figure 1A). We additionally confirmed the low column binding affinity by the standard kinetic activity assay by comparing the activity of the cell lysate with the flow-through, the wash, and the elution fractions. As has been reported previously, a double-hexa-histidine (6xHis-linker-6xHis) tag, connecting two 6xHis tags with an intervening 11-amino acid linker, shows stronger binding to the Ni-NTA surface than a conventional single 6xHis tag.[23] Therefore, we cloned a pTrc12HLB-FdsGBACD vector to encode FdsABG with a double-hexa-histidine (6xHis-linker-6xHis) tag fused to the N-terminus of the FdsG subunit. The affinity chromatography results (Figure 1A) showed that the protein with the 6xHis-linker-6xHis remained on the Ni-NTA column with washing buffer containing 20 mM imidazole and that the protein eluted at >100 mM imidazole.

Previous studies have found that the homologous FdsABG from *R. capsulatus*, heterologously expressed in *E. coli*, yields not only the hexameric $(\alpha\beta\gamma)_2$ FdsABG but also the dimeric $\alpha\beta$ FdsBG, which exhibits significant diaphorase (NADH/O_2 oxidoreductase) activity.[22] We found that this was the case for the *C. necator* system as well, and both FdsABG and FdsBG were expressed during induction of the plasmid with IPTG. Thus, subsequent to Ni-NTA purification, it was necessary to separate the two proteins by size exclusion chromatography using the Superdex 200 (GE Healthcare). The elution fractions from the Ni-NTA column were thus concentrated and loaded onto the size exclusion column. The resulting chromatograph (Figure 1B) showed three major peaks, which correspond to a homodimer of trimers FdsABG $(\alpha\beta\gamma)_2$ with a molecular mass of 358 kDa, a protomer of trimers FdsABG $(\alpha\beta\gamma)$ with a molecular mass of 179 kDa, and an FdsBG $\beta\gamma$ dimer with a molecular mass of 74 kDa. In our hands, there was no correlation in the ratio of monomeric and dimeric protein with variations in growth conditions, pH, protein concentration, etc. Although we find that the monomeric and dimeric forms exhibit indistinguishable catalytic properties, only the dimeric form was used in the present studies. The fractions containing the three major peaks from the size exclusion chromatography were subjected to denaturing SDS-PAGE (Figure 1B). Three

DOI: 10.1021/acs.biochem.8b01301
Biochemistry 2019, 58, 1861−1868

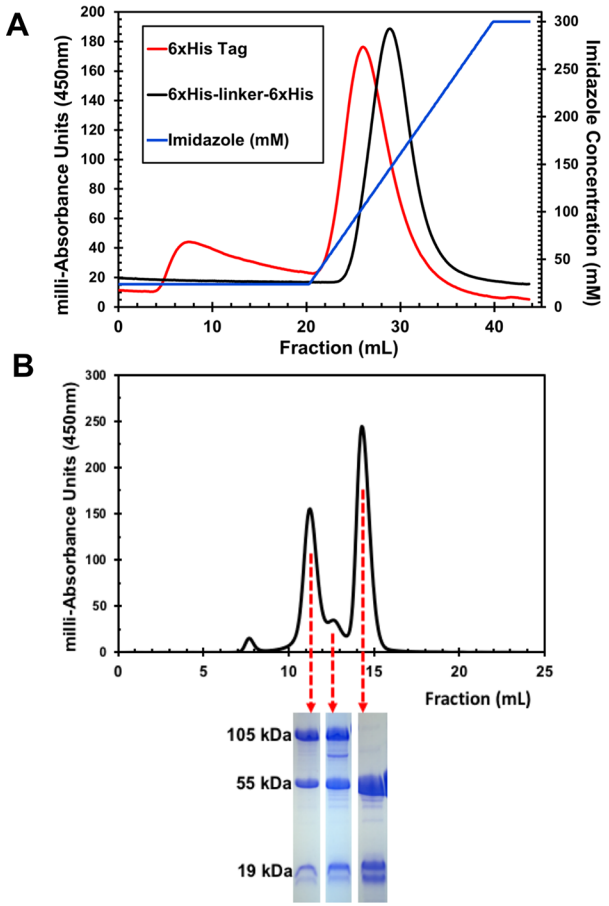

Figure 1. FdsABG purification from *E. coli*. (A) Affinity chromatography and purification of 6xHis-FdsABG (red line) and 6xHis-linker-6xHis-FdsABG (black line) on a Ni-NTA column. The 6xHis-FdsABG showed a first peak from a washing step with 20 mM imidazole and a second peak from a gradient elution with 20−300 mM imidazole (blue line), whereas the 6xHis-linker-6xHis-FdsABG eluted with only one peak at >100 mM imidazole. (B) Size exclusion chromatography and purification of 6xHis-linker-6xHis-FdsABG were performed after Ni-NTA affinity purification. The fractions from each eluted protein peak were collected and concentrated and further analyzed on a 15% denaturing SDS-PAGE. All purification steps were monitored for FdsABG/FdsBG absorbance at 450 nm.

major bands were detected: 105, 55, and 19 kDa, corresponding to subunits FdsA, FdsB, and FdsG, respectively.

To optimize the level of active FdsABG expression, *E. coli* DH5α cells transformed with the pTrc12HLB-FdsGBACD vector were cultured under different growth conditions. In general, higher IPTG concentrations and faster growth rates (as a result of either higher shaking speeds and/or higher temperatures) favored the synthesis of FdsBG. The level of molybdenum cofactor (MGD) saturation has also been reported to be affected by temperature, oxygen tensor, and IPTG concentrations.[22] In general, a slower cell growth attained by low shaking speeds and a lower temperature in combination with low IPTG concentrations for slower protein expression rates favor a higher MGD cofactor saturation. Increasing the molybdate concentration in the growth medium beyond 0.5 mM did not improve the cofactor saturation.

Protein Characterization by EPR Spectroscopy. We next examined the EPR properties of recombinant FdsABG in order to verify that the addition of the 6xHis-linker-6xHis tag to the FdsG subunit perturbed neither the functionality of the enzyme nor the properties of its redox-active centers by examining the recombinant enzyme by EPR. The enzyme was partially reduced with sodium dithionite under anaerobic conditions as previously described[17] and promptly frozen for EPR analysis. The resultant spectrum is presented in Figure 2A

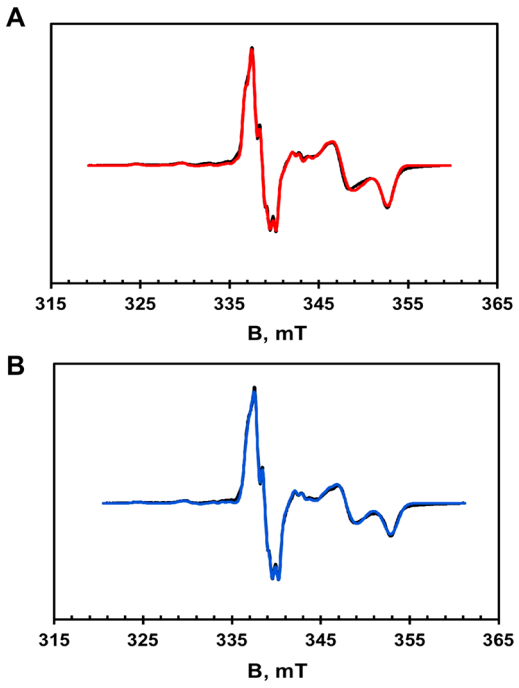

Figure 2. EPR spectroscopy of the Mo center of FdsABG. (A) EPR spectrum (black trace) and simulation (red trace) of the recombinant FdsABG (B) EPR spectrum (black trace) and simulation (red trace) of native FdsABG (reprint by permission, ref 17).

(black trace) with the corresponding simulation below (red trace). For comparison, the spectrum (black trace) and simulation (blue trace) for the native FdsABG are shown in Figure 2B. The spectrum of the recombinant protein is composed of a narrow feature centered around 338 mT arising from the Mo^V species; this signal includes hyperfine coupling due to the 25% naturally occurring $^{95,97}Mo$ (I = 5/2). A second, broad signal is observed that has been attributed to one of the seven Fe/S clusters present in FdsABG[17] (the only Fe/S signal that is observed at 150 K, the temperature at which the data was collected). Simulation of the composite Mo^V−Fe/S spectrum yields g values and proton coupling for the Mo^V contribution to the spectrum in very good agreement with previous reported g(1,2,3) = 2.009, 2.001, 1.992 and (H)A(1,2,3) = 18, 21, 18 MHz,[17] indicating that the molybdenum center is not significantly perturbed by the addition of the 6xHis-linker-6xHis tag. The g values for the Fe/S component of the composite spectrum are also in excellent agreement with the values obtained for the native FdsABG.

Protein Characterization with Kinetic Assays. We have also characterized the recombinant FdsABG by activity assays and compared it with the native enzyme. Native, isolated FdsABG from *C. necator* is a homodimer of trimers, $(\alpha\beta\gamma)_2$, in which the 105 kDa α (FdsA) subunit contains the active site molybdenum center (bis-MGD) where formate is oxidized and CO_2 is reduced, four [4Fe-4S] clusters and a [2Fe-2S] cluster; the 55 kDa β (FdsB) subunit contains a flavin (FMN) cofactor

DOI: 10.1021/acs.biochem.8b01301
Biochemistry 2019, 58, 1861−1868

and a [4Fe-4S] cluster; finally, the 19 kDa γ (FdsG) subunit contains one [2Fe-2S]. The seven iron−sulfur clusters are responsible for the electron transfer within the protein, and the FMN is the site of NAD^+ reduction. The loss of any one of these cofactors during the expression and purification process results in the loss of enzymatic activity as measured by either the formate/NAD^+ or the CO_2/NADH kinetic assays. Therefore, we have used the steady-state kinetic properties of the native, isolated FdsABG from *C. necator* as the standard for characterizing the activity of the recombinant protein.[17,18] The recombinant FdsABG yielded a k_{cat} for formate oxidation of 99 s^{-1} and a k_{cat} for CO_2 reduction of 4.8 s^{-1} under the same experimental conditions as those used for the native enzyme (Figure 3 and Figure 7).[17] By comparing these results with

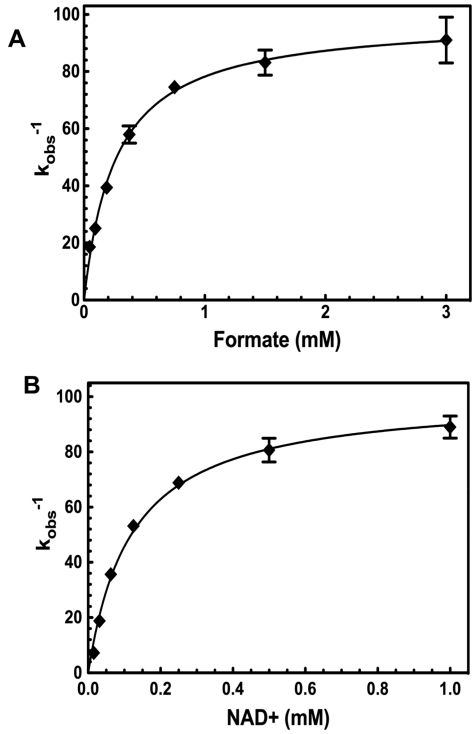

Figure 3. Steady-state kinetic properties of recombinant FdsABG. (A) Hyperbolic plots for the reaction of FdsABG with formate in the presence of 1 mM NAD^+. (B) Hyperbolic plots for the reaction of FdsABG with NAD^+ in the presence of 4 mM formate. Reactions in panels A and B yielded a $K_m^{formate}$ = 260 μM and a K_m^{NAD+} = 110 μM, respectively, and an average k_{cat} of 99 s^{-1}. All reactions were performed in 75 mM KPO_4, pH 7.7, at 30 °C under aerobic conditions.

those for the native FdsABG from *C. necator* (k_{cat} = 11 s^{-1} for CO_2 reduction and k_{cat} = 201 s^{-1} for formate oxidation), we demonstrate that the recombinant FdsABG has been successfully expressed and purified with about 50% functionality. This value is comparable to the ~50% functionality of the native enzyme isolated from *C. necator*, and with that seen in other heterologous expressions systems for other MGD cofactor-containing enzymes,[22] indicating that our *E. coli* recombinant system is just as effective as the native *C. necator* in incorporating the molybdenum center into apoprotein.

Production of Formate with Fixation of CO_2 Based on Enzymatic Regeneration of NADH. The biotechnology sector and energy sector have brought great attention to utilizing formate dehydrogenase (FDH) to catalyze CO_2 to formate, as this solves two problems, excess emission of CO_2 and depletion of fossil fuels, in a single process. However, the major challenge in working with most FDHs is their intolerance to O_2 and low turnover rates in catalyzing the *in vitro* reduction of CO_2. To extend the analysis of the ability of the recombinant FdsABG to catalyze CO_2 to formate, we have combined FdsABG with a glucose dehydrogenase (GDH) in a cascade reaction; Figure 4 presents the schematic for this

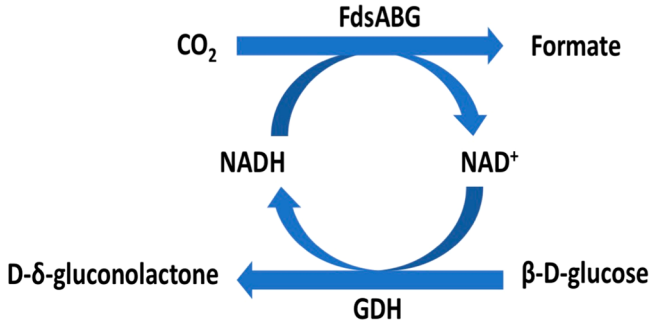

Figure 4. Schematic illustration of the enzymatic cascade reaction involving FdsABG and GDH. FdsABG catalyzes the conversion of carbon dioxide to formic acid, while NADH is oxidized to NAD^+. GDH catalyzes the conversion of β-D-glucose to D-δ-gluconolactone, while NAD^+ from the FdsABG reaction is reduced to NADH.

process. The enzyme GDH catalyzes the oxidation of glucose to gluconolactone and in the process generates two protons and two electrons, which are used to reduce NAD^+ to NADH (eq 1), and subsequently FdsABG.

$$\beta\text{-D-glucose} + NAD^+ \rightarrow \text{D-}\delta\text{-gluconolactone} + NADH + H^+ \quad (1)$$

To investigate the suitability of GDH for the cascade reaction, we first performed a steady-state analysis of the enzyme under the optimum reaction conditions for the recombinant FdsABG (30 °C, 1 atm, pH 7.0). As shown in Figure 5, the results were plotted according to the Michaelis−Menten equation and yielded hyperbolic relationships from which kinetic parameters could be extracted. A k_{cat} of 200 s^{-1} and a $K_m^{glucose}$ of 2.7 mM (Figure 5a) and a K_m^{NAD+} of 120 μM at pH 7.0 (Figure 5b) were thus obtained.

Next, we combined GDH and FdsABG in a ratio that reflects similar activities (based on k_{cat} values at pH 7.0) to promote a continuous electron transfer for the reaction, in which CO_2 is converted to formate. In this experiment, samples were removed at different time points after addition of both FdsABG and GDH, and formate was quantified by ion chromatography, as we have previously reported.[18] In this earlier work, we have also confirmed formate as the sole product by ^{13}C NMR, using C^{13}-labeled CO_2 gas as a reaction substrate. This work not only confirmed the formation of formate but also demonstrated the sensitivity and accuracy of ion chromatography for the quantitative analysis of formate.

As shown in Figure 6, in one group of experiments (blue squares), we used substrate concentrations that were saturating for both enzymes: 20 mM glucose, 0.5 mM NAD^+, and 28 mM dissolved CO_2 gas at 30 °C, 1 atm, pH 7.0. We found that formate accumulated quickly after the reaction was initiated, but the rate would slow down dramatically after 4 h. Additionally, the formate concentration stalled at 1 mM even after 10 h of reaction time. There are a number of possible reasons for the reaction plateau including enzyme inactivation, substrate limitation, and production inhibition of FdsABG. To

DOI: 10.1021/acs.biochem.8b01301
Biochemistry 2019, 58, 1861−1868

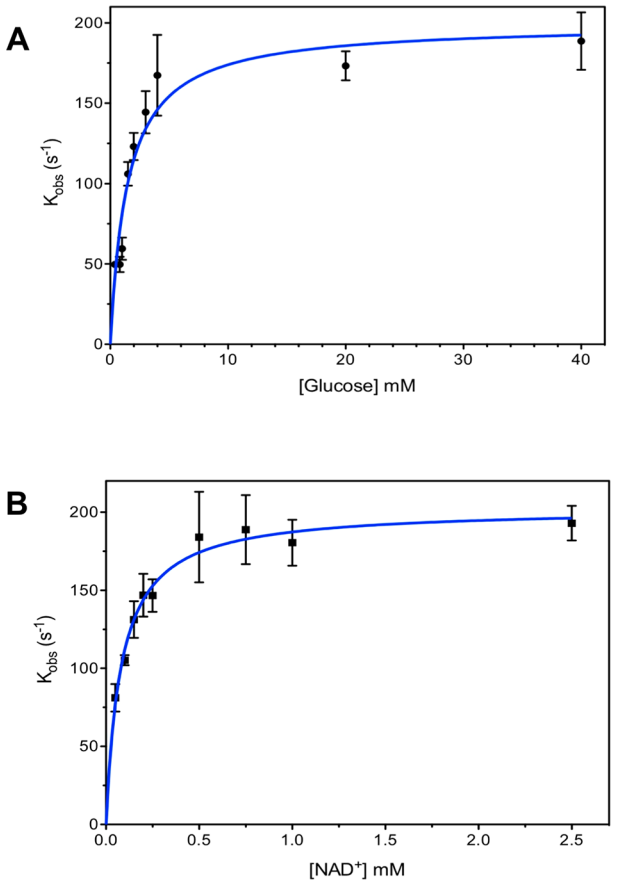

Figure 5. Steady-state kinetic properties of GDH. (A) Hyperbolic plots for the reaction of GDH with glucose in the presence of 2 mM NAD^+. (B) Hyperbolic plots for the reaction of FdsABG with NAD^+ in the presence of 40 mM glucose. Reactions in panels A and B yielded a $K_m^{glucose}$ = 2.7 mM and a K_m^{NAD+} = 120 μM, respectively, and an average k_{cat} of 200 s^{-1}. All reactions were performed in 100 mM KPO_4, pH 7.0, at 30 °C under anaerobic conditions.

distinguish between these possibilities, we performed several reactions and steady-state experiments whose results are presented in Figures 6 and 7. To test for the inactivation of one or both of the enzymes during the progress of the 10 h reaction, a similar amount of GDH and FdsABG was introduced at 2 h after the reaction was started (Figure 6, green triangles). Additional enzyme, however, only marginally improved the production of formate; the maximum concentration still did not exceed 1.1 mM. We also tested the effect of varying the glucose concentration on the yield of formate after a 10 h reaction period. Under the conditions of saturated CO_2 (28 mM) and NAD^+ (0.5 mM), 4 mM of glucose yielded only 0.2 mM formate (Figure 6, pink squares), while the increase of glucose to 50 mM (Figure 6, red squares) did not yield any more formate than the 20 mM glucose used in the previous experiments. We also decreased the NAD^+ concentration to 0.2 mM (Figure 6, yellow squares), under the same conditions as above with a result that formate production decreased to 0.7 mM after the 10 h incubation. Finally, we performed a series of steady-state experiments with a saturated solution of CO_2 and 0.2 mM NADH in the presence of 0−1.5 mM formate to test for product inhibition of FdsABG (Figure 7). The data indicated that the $k_{cat(app)}^{CO_2}$ was dramatically affected by the presence of formate, decreasing to 22% in the presence of 1.5 mM of the product. We have also verified that the pH of the

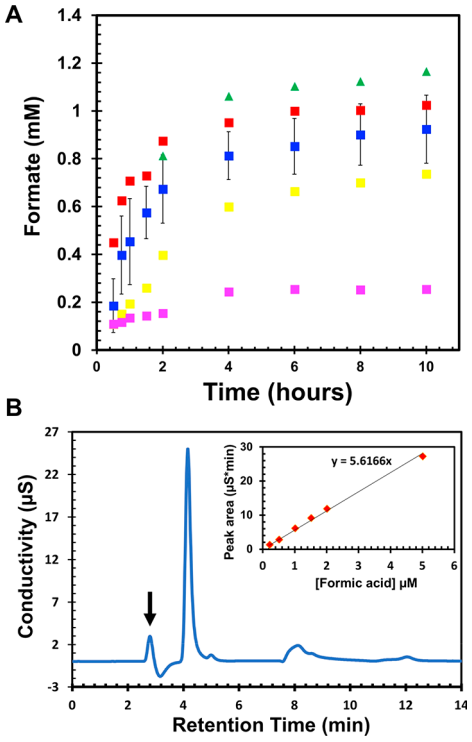

Figure 6. (A) Plots of formate production as a function of reaction time for the enzymatic cascade reaction involving FdsABG and GDH. Reactions of FdsABG and GDH with 28 mM dissolved CO_2 gas, 0.5 mM NAD^+, and 20 mM glucose (blue square), 4 mM of glucose (pink square), or 50 mM glucose (red square). Additional enzymes were introduced to the blue square group at 2 h after the reaction was started (green triangle). Reactions of FdsABG and GDH with 28 mM dissolved CO_2 gas, 0.2 mM NAD^+, and 20 mM glucose (yellow square). All reactions were measured by ion chromatography for the accumulation of formate, and all reactions were performed in 20 mM bis-tris buffer at pH 7.0 and 30 °C. (B) An example of an ion chromatogram for formate analysis of the reaction in panel A. The black arrow indicates the formate peak at a retention time of 3.9 min. A standard calibration curve of formate is in the inset of panel B.

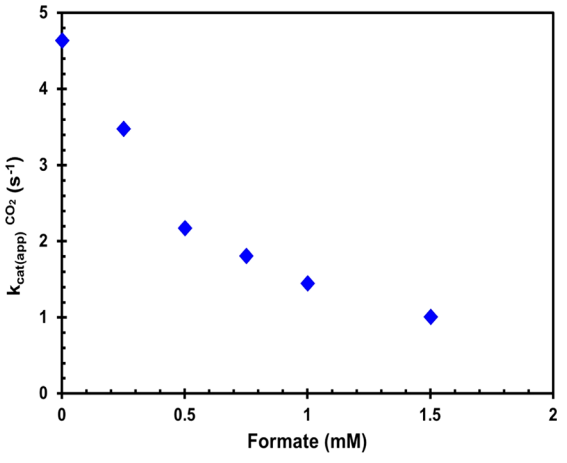

Figure 7. Inhibition effect of formate concentration on the reaction of FdsABG on with 200 μM NADH and saturated (28 mM) CO_2 (aq). The reaction of recombinant FdsABG with CO_2 and no initial formate yielded a $k_{cat(app)}^{CO_2}$ of 4.7 s^{-1}. As the initial concentration of formate increased, the $k_{cat(app)}^{CO_2}$ for recombinant FdsABG dropped. All reactions were performed in 100 mM KPO_4 buffer at pH 7.0 and 30 °C under anaerobic conditions.

DOI: 10.1021/acs.biochem.8b01301
Biochemistry 2019, 58, 1861−1868

reaction is unchanged in the course of the reaction for the experiments shown in Figures 6 and 7. The implication of the above experiments is that product inhibition (an effect on K_m) is the major reason for the rate decreases and eventual stagnation in the yield of formate in the cascade reaction. Thus, for production of formate with FdsABG at a maximum rate, the product would need to be continuously removed to a level below 0.4 mM for maintaining the reaction of CO_2 reduction catalyzed by FdsABG at a relatively high rate.

According to the reaction scheme in Figure 4, we have run an enzyme cascade reaction involving two enzymes: FdsABG to oxidize NADH to NAD^+ and GDH to reduce NAD^+ back to NADH. Given the overall stoiochiometry of NADH oxidation and formate reduction, we can define an effective total turnover number with respect to NADH according to the following eq 2:

$$\text{effective TTN} = \frac{C_{\text{formate,t}}}{C_{\text{NADH,initial}}} \quad (2)$$

The NADH-based formate yield of the reaction was calculated based on the percentage of formate production concentration (0.9 mM) divided by the initiation concentration of NADH (0.5 mM). The total yield is about 180%, which corresponds to an effective TTN of NADH of 1.8. This effective TTN for NADH demonstrates that the reaction system effectively utilizes NADH as an electron source for the reduction of CO_2 reduction.

In comparison to previous studies on FDHs for CO_2 reduction,[9,21] our results indicate that our recombinant *C. necator* FdsABG is effecitve in the reduction of CO_2 to formate, with an effective TTN of 1.8 for NADH in the presence of the glucose/glucose dehydrogenase system for regeneration of NADH. We emphasize that the observed value of 1.8 is not limited by the exhaustion of the NADH regeneration system, but rather by the accumulation of product formate; it is greatly improved over the effective TTN of 0.2 observed in the absence of the NADH regeneration system.[18] Our results thus constitute an important proof-of-principle demonstration that the glucose/glucose dehydrogenase NADH regeneration system is indeed an effective means by which CO_2 reduction can be enhanced in an enzyme-catalyzed system.

CONCLUSIONS

In this study, we have successfully cloned the full-length soluble formate dehydrogenase (FdsABG) from *C. necator* and heterologously expressed and purified from *E. coli* with a 6xHis-linker-6xHis tag fused to the N terminus of the FdsG subunit. We have also characterized the recombinant FdsABG with EPR spectroscopy as well as kinetic assays and compared it with the native, isolated FdsABG from *C. necator*. As expected, the recombinant FdsABG has about 50% functionality compared with the native isolated one.

We have further combined this recombinant *C. necator* FdsABG with another enzyme, glucose dehydrogenase, for continuous regeneration of NADH in converting CO_2 to formate. The recombinant *C. necator* FdsABG examined here has considerable potential for industrial applications due to its air stability, and the demonstration here that coupling with the NADH regenerating system glucose/glucose dehydrogenase significantly enhances CO_2 reduction, even in the absence of product (formate) removal, is promising for the development of increasingly efficient biocatalytic processes for CO_2 fixation. Still, considerable work remains to be done in the development of an industrially feasible process for CO_2 fixation that is based on the CO_2 reductase activity of FdsABG, including, for example, the development of a means for the removal of the product, formic acid, from the reaction mix in order to prevent product inhibition of the enzyme. Nevertheless, the present work does constitute an important proof-of-principle demonstration of the effectiveness of the glucose/glucose dehydrogenase system in regenerating NADH for repeated use in CO_2 reduction and provides a framework for studying electron transfer inside this protein as well the development of highly efficient CO_2 biocatalytic fuel cells.

ASSOCIATED CONTENT

Accession Codes

FdsA, Q0KDY1; FdsB, Q0KDY2; FdsG, Q0KDY3.

AUTHOR INFORMATION

Corresponding Authors

*E-mail: russ.hille@ucr.edu.
*E-mail: adani@engr.ucr.edu.

ORCID

Xuejun Yu: 0000-0002-2879-8881
Xin Ge: 0000-0001-7491-7805
Haizhou Liu: 0000-0003-4194-2566
Ashok Mulchandani: 0000-0002-2831-4154

Notes

The authors declare no competing financial interest.

ACKNOWLEDGMENTS

This work was supported by the National Science Foundation (NSF-CBET 1265044 to A.M.) and the Department of Energy (DE-SC0010666 to R.H.).

REFERENCES

(1) Appel, A. M., Bercaw, J. E., Bocarsly, A. B., Dobbek, H., DuBois, D. L., Dupuis, M., Ferry, J. G., Fujita, E., Hille, R., Kenis, P. J. A., Kerfeld, C. A., Morris, R. H., Peden, C. H. F., Portis, A. R., Ragsdale, S. W., Rauchfuss, T. B., Reek, J. N. H., Seefeldt, L. C., Thauer, R. K., and Waldrop, G. L. (2013) Frontiers, Opportunities, and Challenges in Biochemical and Chemical Catalysis of CO_2 Fixation. *Chem. Rev.* *113* (8), 6621−6658.

(2) Enthaler, S., von Langermann, J., and Schmidt, T. (2010) Carbon dioxide and formic acid-the couple for environmental-friendly hydrogen storage? *Energy Environ. Sci.* *3* (9), 1207−1217.

(3) Sordakis, K., Tang, C. H., Vogt, L. K., Junge, H., Dyson, P. J., Beller, M., and Laurenczy, G. (2018) Homogeneous Catalysis for Sustainable Hydrogen Storage in Formic Acid and Alcohols. *Chem. Rev.* *118* (2), 372−433.

(4) Yadav, M., and Xu, Q. (2012) Liquid-phase chemical hydrogen storage materials. *Energy Environ. Sci.* *5* (12), 9698−9725.

(5) Shi, J. F., Jiang, Y. J., Jiang, Z. Y., Wang, X. Y., Wang, X. L., Zhang, S. H., Han, P. P., and Yang, C. (2015) Enzymatic conversion of carbon dioxide. *Chem. Soc. Rev.* *44* (17), 5981−6000.

(6) Zhong, H., Iguchi, M., Chatterjee, M., Himeda, Y., Xu, Q., and Kawanami, H. (2018) Formic Acid-Based Liquid Organic Hydrogen Carrier System with Heterogeneous Catalysts. *Advanced Sustainable Systems* *2* (2), 1700161.

(7) Qiao, J., Liu, Y., Hong, F., and Zhang, J. (2014) A review of catalysts for the electroreduction of carbon dioxide to produce low-carbon fuels. *Chem. Soc. Rev.* *43* (2), 631−675.

(8) Maia, L. B., Moura, J. J. G., and Moura, I. (2015) Molybdenum and tungsten-dependent formate dehydrogenases. *JBIC, J. Biol. Inorg. Chem.* *20* (2), 287−309.

DOI: 10.1021/acs.biochem.8b01301
Biochemistry 2019, 58, 1861−1868

(9) Maia, L. B., Moura, I., and Moura, J. J. G. (2017) Molybdenum and tungsten-containing formate dehydrogenases: Aiming to inspire a catalyst for carbon dioxide utilization. *Inorg. Chim. Acta 455*, 350−363.
(10) Choe, H., Joo, J. C., Cho, D. H., Kim, M. H., Lee, S. H., Jung, K. D., and Kim, Y. H. (2014) Efficient CO_2-Reducing Activity of NAD-Dependent Formate Dehydrogenase from *Thiobacillus* sp KNK65MA for Formate Production from CO_2 Gas. *PLoS One 9* (7), e103111.
(11) El-Zahab, B., Donnelly, D., and Wang, P. (2008) Particle-tethered NADH for production of methanol from CO_2 catalyzed by coimmobilized enzymes. *Biotechnol. Bioeng. 99* (3), 508−514.
(12) Yadav, R. K., Baeg, J.-O., Oh, G. H., Park, N.-J., Kong, K.-j., Kim, J., Hwang, D. W., and Biswas, S. K. (2012) A Photocatalyst-Enzyme Coupled Artificial Photosynthesis System for Solar Energy in Production of Formic Acid from CO_2. *J. Am. Chem. Soc. 134* (28), 11455−11461.
(13) Kim, S., Kim, M. K., Lee, S. H., Yoon, S., and Jung, K.-D. (2014) Conversion of CO_2 to formate in an electroenzymatic cell using Candida boidinii formate dehydrogenase. *J. Mol. Catal. B: Enzym. 102*, 9−15.
(14) Srikanth, S., Maesen, M., Dominguez-Benetton, X., Vanbroekhoven, K., and Pant, D. (2014) Enzymatic electrosynthesis of formate through CO_2 sequestration/reduction in a bioelectrochemical system (BES). *Bioresour. Technol. 165*, 350−354.
(15) de Bok, F. A. M., Hagedoorn, P. L., Silva, P. J., Hagen, W. R., Schiltz, E., Fritsche, K., and Stams, A. J. M. (2003) Two W-containing formate dehydrogenases (CO_2-reductases) involved in syntrophic propionate oxidation by Syntrophobacter fumaroxidans. *Eur. J. Biochem. 270* (11), 2476−2485.
(16) Oh, J. I., and Bowien, B. (1998) Structural analysis of the fds operon encoding the NAD(+)-linked formate dehydrogenase of Ralstonia eutropha. *J. Biol. Chem. 273* (41), 26349−26360.
(17) Niks, D., Duvvuru, J., Escalona, M., and Hille, R. (2016) Spectroscopic and Kinetic Properties of the Molybdenum-containing, NAD(+) - dependent Formate Dehydrogenase from Ralstonia eutropha. *J. Biol. Chem. 291* (3), 1162−1174.
(18) Yu, X. J., Niks, D., Mulchandani, A., and Hille, R. (2017) Efficient reduction of CO_2 by the molybdenum-containing formate dehydrogenase from Cupriavidus necator (Ralstonia eutropha). *J. Biol. Chem. 292* (41), 16872−16879.
(19) Weckbecker, A., Groeger, H., and Hummel, W. (2010) Regeneration of Nicotinamide Coenzymes: Principles and Applications for the Synthesis of Chiral Compounds. *Biosystems Engineering I: Creating Superior Biocatalysts 120*, 195−242.
(20) Addo, P. K., Arechederra, R. L., Waheed, A., Shoemaker, J. D., Sly, W. S., and Minteer, S. D. (2011) Methanol Production via Bioelectrocatalytic Reduction of Carbon Dioxide: Role of Carbonic Anhydrase in Improving Electrode Performance. *Electrochem. Solid-State Lett. 14* (4), E9−E13.
(21) Ji, X., Su, Z., Wang, P., Ma, G., and Zhang, S. (2015) Tethering of Nicotinamide Adenine Dinucleotide Inside Hollow Nanofibers for High-Yield Synthesis of Methanol from Carbon Dioxide Catalyzed by Coencapsulated Multienzymes. *ACS Nano 9* (4), 4600−4610.
(22) Hartmann, T., and Leimkuehler, S. (2013) The oxygen-tolerant and NAD(+)-dependent formate dehydrogenase from Rhodobacter capsulatus is able to catalyze the reduction of CO_2 to formate. *FEBS J. 280* (23), 6083−6096.
(23) Khan, F., He, M. Y., and Taussig, M. J. (2006) Double-hexahistidine tag with high-affinity binding for protein immobilization, purification, and detection on Ni-nitrilotriacetic acid surfaces. *Anal. Chem. 78* (9), 3072−3079.

DOI: 10.1021/acs.biochem.8b01301
Biochemistry 2019, 58, 1861−1868